Damage mechanisms of composite laminates under impact loading including the effect of pre-load

Wenxin Zhang [a], Di Zhang [a], Jin Zhou [a,*], Jiangwei Qi [a], Wen Zhao [a], Shuming Yang [a], John P. Dear [b], Haibao Liu [c,*]

[a] School of Mechanical Engineering, Xi'an Jiaotong University, Xi'an 710049, China

[b] Department of Mechanical Engineering, Imperial College London, London, SW7 2AZ, UK

[c.] School of Engineering and Materials Science, Queen Mary University of London, London E1 4NS, UK

* Corresponding emails: jin.zhou@xjtu.edu.cn (J. Zhou), haibao.liu@qmul.ac.uk (H. Liu).

Abstract

The focus of the present research is on the damage modelling of composite laminates subjected to Low Velocity Impact (LVI). This research also shows how this model can be employed to assess the effect of pre-load. The composite damage model, integrating a VUMAT subroutine and a cohesive zone model, is first validated against the results obtained from conventional impacts on laminates without pre-load. The validated model is then employed to predict the impact response of pre-loaded composite laminates. It was found that the pre-load influences the load response, damage behaviour and energy absorption mechanisms of composite laminates. This is with pre-tension increases the maximum load during the impact event, whereas pre-compression has the opposite effect. Matrix cracking and delamination are found to be reduced slightly due to pre-tension, whilst matrix cracking and delamination are considerably increased by pre-compression. The developed model can provide guidance to the design and maintenance of composite components subjected to pre-load and impact.

Keywords: Composite laminates; Pre-load; Impact damage; Numerical simulation.

1 Introduction

Composites are attractive for commercial aircraft structures due to their high specific strength and stiffness, as well as excellent fatigue and corrosion resistance [1-4]. However, when employed in fuselage and wing structures, composite materials may encounter a variety of impact threats during their service [5-8]. In particular, impact damage can reduce structural integrity significantly. To better understand and predict the impact performance of composite materials, researchers have performed experimental studies and numerical simulation on well-defined impact geometries [9-13]. Xu et al. [10] emphasised the importance of indentation mechanics in the impact event. This is important in determining the upper limit of interlaminar damage in composite laminates and providing a way of predicting the damage tolerance of composite materials under low velocity impact (LVI). It was found that that predicted results tend to be very conservative, especially for thick composite laminates. Liu et al. [12] predicted the overall impact behaviour of composite materials accurately through a three-dimensional finite element analysis (FEA) model by considering the elastic-plastic behaviour of composites. The load-deflection response, initiation and propagation of intralaminar damage (matrix cracking) and interlaminar damage (delamination) processes were analysed in detail.

For aircraft structures which see aerodynamic loading, pre-stress before impact is an important consideration [14, 15]. When aircraft is on the ground, upper wing skin is subjected to tension and lower skin is subjected to compression load. When the aircraft is in maneuvre, fuselage skin may be subjected to tensile load due to pressurisation, upper wing skin is subjected to compression and lower wing skin is subjected to tension. These loads will be unavoidably applied to the structures as pre-loads before any damage loads come into effects. For this reason, where possible, the effect of pre-load should be assessed when doing impact testing of an aircraft structural components [16, 17]. As early as 1991, the importance of the effects of pre-stress were highlighted in a NASA symposium [18, 19]. Several leading European researchers have noted that pre-load can affect matrix cracking and delamination damage and this has been noted in the Federal Aviation Administration (FAA) Advisory Circular [20, 21]. These and other researchers have noted, through experimental and numerical studies, that pre-load in a fibre direction of a particular lamina can lead to matrix tensile cracking, due to Poisson's effect, so increasing delamination [22-24].

Guillaud et al. [25] focussed on the impact response of carbon/epoxy composites laminates subjected to uniaxial pre-tension. When pre-tension was applied, the cumulative area of delamination increased. The maximum displacement decreases and the maximum load of the sample increases as the pre-load increases. Also, the energy absorption rate is greater for high pre-load and a low impact energy. Hu et al. [26-28] designed and developed a new pre-loading device (uniaxial tension and uniaxial compression) for the LVI test of composite laminates. The results showed that the application of pre-load during LVI of composite laminates, not only changes the impact response, but also changes the energy absorption mode. The impact damage in hybrid woven laminates under tensile or compressive pre-load was mainly manifested as delamination and fibre tensile failure. Khalili and Choi et al. [29, 30] used Sveklo's contact theory and a modified displacement field to study LVI response on pre-loaded orthotropic laminates.

Kursun et al. [31] investigated the influence of biaxial pre-load on the LVI performance of E-glass/epoxy-laminated composite by experiments and simulations. The deflection of the laminates increased with the effect of pre-load, and energy absorption exhibited a similar trend. Therefore, composite material damage with a pre-compression load was higher than that when the laminate was not pre-loaded. Ruivo Fuga et al. [32] studied the LVI response of woven carbon fibre composite laminates and developed a continuum damage mechanics (CDM) constitutive model to verify its correlation from low strain level to the post-buckling condition. Results from both the experiments and the simulations showed that the in-plane damage is the main type of damage. The higher pre-load levels tended to cause more serious damage. In addition, analytical and numerical modelling predictions for delamination damage were compared to the experimental contact load histories. The results showed that the threshold load for delamination was related to the intralaminar damage. Rathnasabapathy et al. [33-35] experimentally investigated the effect of in-plane load on the LVI damage tolerance of Fibre Metal Laminate (FML). When the FMLs were subjected to LVI, the plastic deformation and delamination damage increase with the increase of the pre-strain. Moreover, the finite element model predicted the effects of pre-loads on the plastic damage of bulk deformed metal plates and the delamination of composite laminates.

Other researchers have employed complex biaxial loading rigs, different frontal geometries for LVI and even high velocity ballistic impacts and they have observed similar effects on damage due to preload [36-42].

In summary, several researchers have studied the effect of LVI of composite laminates under pre-load and observed experimentally that matrix cracking and delamination increase with pre-load and this effect is more marked under compressive pre-loading. With these experimental findings in mind, it is thought there is scope to understand better, through modelling, the influence of pre-load on impact failure mechanisms and associated energy dissipation in composites. In this paper, a three-dimensional progressive damage model, consisting of a VUMAT subroutine and a cohesive zone model, was developed to predict the LVI damage and energy absorption behaviour of carbon fibre/epoxy composite laminates subjected to different type of pre-load conditions. The effects of pre-load on LVI performance of the composite laminates are discussed in detail, concentrating on load response and impact-induced damage. More importantly, from a new perspective, the effect of pre-load on energy absorption mechanisms of composite laminates during the LVI event has been investigated.

2 Composite damage model

Failure mechanisms of composite laminates under LVI are usually divided into two main types: intralaminar damage and interlaminar damage, i.e. delamination. Intralaminar damage, which occurs within composite plies, includes fibre tension and compression failure as well as matrix tension and compression cracking. Interlaminar damage reflects delamination between composite plies. In this work, a three-dimensional progressive damage model has been implemented with Fortran-coded 'VUMAT' subroutine to capture the intralaminar damage. Correspondingly, a cohesive zone model has been employed to predict the interlaminar damage, i.e. delamination.

2.1 Intralaminar damage model

Generally, composites can be considered as homogeneous and transversely isotropic materials, for which a transversely isotropic constitutive equation with five independent constants can be employed for the pristine lamina. The modified 3D Hashin failure criteria [43, 44] are used to capture the intralaminar damage initiation in composite laminates, given as follows:

(1) Fibre failure in tension（$\sigma_{11} \geq 0$）:

$$\left(\frac{\sigma_{11}}{X_{\mathrm{T}}}\right)^2 + \left(\frac{\sigma_{12}}{S_{12}}\right)^2 + \left(\frac{\sigma_{13}}{S_{13}}\right)^2 \geq 1 \tag{1}$$

(2) Fibre failure in compression（$\sigma_{11} < 0$）:

$$\left(\frac{\sigma_{11}}{X_{\mathrm{C}}}\right)^2 \geq 1 \tag{2}$$

(3) Matrix failure in tension（$\sigma_{22}+\sigma_{33} \geq 0$）:

$$\left(\frac{\sigma_{22}+\sigma_{33}}{Y_{\mathrm{T}}}\right)^2 + \left(\frac{\sigma_{12}}{S_{12}}\right)^2 + \left(\frac{\sigma_{13}}{S_{13}}\right)^2 + \frac{1}{S_{23}^2}\left(\sigma_{23}^2 - \sigma_{22}\sigma_{33}\right) \geq 1 \tag{3}$$

(4) Matrix failure in compression（$\sigma_{22}+\sigma_{33} < 0$）:

$$\left(\frac{\sigma_{22}+\sigma_{33}}{2S_{23}}\right)^2 + \left(\frac{\sigma_{12}}{S_{12}}\right)^2 + \left(\frac{\sigma_{13}}{S_{13}}\right)^2 + \frac{1}{S_{23}^2}\left(\sigma_{23}^2 - \sigma_{22}\sigma_{33}\right) + \frac{\sigma_{22}+\sigma_{33}}{Y_{\mathrm{C}}}\left[\left(\frac{Y_C}{2S_{23}}\right)^2 - 1\right] \geq 1 \tag{4}$$

where, $\sigma_{ij\ (i,j=1,2,3)}$ represents effective stress tensor, X_{T}、X_{C}、Y_{T}、Y_{C} are the tensile and compressive strengths of composites along to and perpendicular to the longitudinal direction, respectively. S_{12}、S_{13}、S_{23} are shear strengths in the three directions, respectively.

After the intralaminar damage initiation, cracks propagate within the composite materials, which lead to the degradation of material property. Therefore, damage variables are introduced to account for the materials degeneration during subsequent progressive stage. The modified constitutive equations have been used to describe the stress-strain relationship for the damaged composite lamina. Through the degraded stiffness matrix, C_d, the stress-strain relationship after the onset of intralaminar damage is given as:

$$\sigma = C_d \varepsilon \tag{5}$$

Fig. 1 shows the bilinear traction-separation law for the intralaminar damage evolution in unidirectional composites. The general form of the damage variable, d, is expressed as:

$$d=\frac{\varepsilon^{f}\left(\varepsilon-\varepsilon^{0}\right)}{\varepsilon\left(\varepsilon^{f}-\varepsilon^{0}\right)} \tag{6}$$

where ε is the current strain of composite materials. Terms ε^0 and ε^f are the initial damage strain and the final failure strain, respectively. The strain expression of final failure is given by:

$$\varepsilon_{ij}^{f}=\frac{2G_c\big|_{ij}}{\sigma_{ij}^{0}} \tag{7}$$

where, $G_c\big|_{ij}$ refers to $G_{\mathrm{Ic}}\big|_{ft}$ 、$G_{\mathrm{Ic}}\big|_{fc}$ 、$G_{\mathrm{Ic}}\big|_{mt}$ 、$G_{\mathrm{Ic}}\big|_{mc}$, representing the intralaminar fracture energies of tension and compression in the longitudinal direction and the transverse direction. The term σ_{ij}^{0} stands for the stress corresponding to the onset of damage.

Satisfying the above equation means the damage initiation and further increase in load and damage propagation. Introducing a characteristic length (L_c) defines how damage propagates based on the displacement instead of strain to reduce the dependency of mesh [45]. Therefore, Equation (6) could be also represented as:

$$d=\frac{\delta^{f}\left(\delta-\delta^{0}\right)}{\delta\left(\delta^{f}-\delta^{0}\right)} \tag{8}$$

where, δ, δ^0, δ^f represent equivalent displacement in fracture according to the associated fracture mode, equivalent displacement of damage initiation, and equivalent displacement of failure.

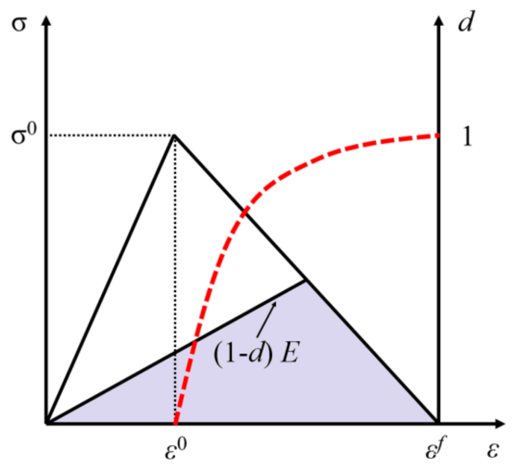

Fig. 1 Bilinear traction-separation law for the intralaminar damage evolution.

Through the VUMAT subroutine, the equivalent stress and displacement of intralaminar damage are presented, including the tensile and compressive damage of fibre and matrix, which are given below. In this study, $\langle\ \rangle$ indicates the Macaulay operator, which is expressed as

$\langle x \rangle = \frac{x+|x|}{2}$. In this model, L_c =0.25mm, which is the thickness of each ply of composites.

Fibre tension：

$$\delta_{ft,eq} = L_c \sqrt{\langle \varepsilon_{11} \rangle^2 + \varepsilon_{12}^2 + \varepsilon_{13}^2} \tag{9}$$

$$\sigma_{ft,eq} = \frac{L_c \left(\langle \sigma_{11} \rangle \langle \varepsilon_{11} \rangle + \sigma_{12}\varepsilon_{12} + \sigma_{13}\varepsilon_{13} \right)}{\delta_{ft,eq}} \tag{10}$$

Fibre compression：

$$\delta_{fc,eq} = L_c \langle -\varepsilon_{11} \rangle \tag{11}$$

$$\sigma_{fc,eq} = \frac{L_c \langle -\sigma_{11} \rangle \langle -\varepsilon_{11} \rangle}{\delta_{fc,eq}} \tag{12}$$

Matrix tension：

$$\delta_{mt,eq} = L_c \sqrt{\langle \varepsilon_{22} \rangle^2 + \langle \varepsilon_{33} \rangle^2 + \varepsilon_{12}^2 + \varepsilon_{23}^2 + \varepsilon_{13}^2} \tag{13}$$

$$\sigma_{mt,eq} = \frac{L_c \left(\langle \sigma_{22} \rangle \langle \varepsilon_{22} \rangle + \langle \sigma_{33} \rangle \langle \varepsilon_{33} \rangle + \sigma_{12}\varepsilon_{12} + \sigma_{23}\varepsilon_{23} + \sigma_{13}\varepsilon_{13} \right)}{\delta_{mt,eq}} \tag{14}$$

Matrix compression：

$$\delta_{mc,eq} = L_c \sqrt{\left(\langle -\varepsilon_{22} \rangle^2 + \langle -\varepsilon_{33} \rangle^2 + \varepsilon_{12}^2 + \varepsilon_{23}^2 + \varepsilon_{13}^2 \right)} \tag{15}$$

$$\sigma_{mc,eq} = \frac{L_c \left(\langle -\sigma_{22} \rangle \langle -\varepsilon_{22} \rangle + \langle -\sigma_{33} \rangle \langle -\varepsilon_{33} \rangle + \sigma_{12}\varepsilon_{12} + \sigma_{23}\varepsilon_{23} + \sigma_{13}\varepsilon_{13} \right)}{\delta_{mc,eq}} \tag{16}$$

During the evolution of intralaminar damage, the degraded stress values can be calculated through the degradation stiffness matrix and materials strain. Damage variables, d_{mc}, d_{mt}, d_{fc} and d_{ft}, which vary from ‘0’ to ‘1’, reflect matrix compression damage, matrix tension damage, fibre compression damage and fibre tension damage, respectively, are given by,

$$d_f = \begin{cases} d_{ft} & \text{if } \sigma_{11} \geq 0 \\ d_{fc} & \text{if } \sigma_{11} < 0 \end{cases} \tag{17}$$

$$d_m = \begin{cases} d_{mt} & \text{if } \sigma_{22} \geq 0 \\ d_{mc} & \text{if } \sigma_{22} < 0 \end{cases} \tag{18}$$

When the value of damage variables d_m and d_f are 0, it means the damage initiates. While when the values of these damage variables equal to 1, it indicates that the material unit has failed completely. The degraded stiffness matrix C_d, which is updated using the damage variable d, is given by:

$$C_d = \frac{1}{D}\begin{bmatrix} dC_{11} & dC_{12} & dC_{13} & 0 & 0 & 0 \\ dC_{21} & dC_{22} & dC_{23} & 0 & 0 & 0 \\ dC_{31} & dC_{32} & dC_{33} & 0 & 0 & 0 \\ 0 & 0 & 0 & dC_{44} & 0 & 0 \\ 0 & 0 & 0 & 0 & \mathrm{dC}_{55} & 0 \\ 0 & 0 & 0 & 0 & 0 & \mathrm{dC}_{66} \end{bmatrix} \tag{19}$$

where

$$D = 1 - d_f d_m \upsilon_{12}\upsilon_{21} - d_m \upsilon_{23}\upsilon_{32} - d_f \upsilon_{31}\upsilon_{13} - 2d_f d_m \upsilon_{21}\upsilon_{32}\upsilon_{13} \tag{20}$$

$$d_f = \left(1 - d_{ft}\right)\left(1 - d_{fc}\right) \tag{21}$$

$$d_m = \left(1 - S_{mt} d_{mt}\right)\left(1 - S_{mc} d_{mc}\right) \tag{22}$$

In the above expressions, S_{mc} and S_{mt} are the shear stiffness degradation variables of the matrix under tension and compression, controlling shear stiffness degradation due to matrix damage. The work performed by Liu et al. [46] and Zhou et al. [47] indicated that these shear stiffness degradation variables need to be calibrated for different types of materials. In this research, the value of 0.96 was finally determined for S_{mc} and S_{mt} based on the coefficient calibration. Material parameters requested for the presented composite damage model, which obtained from the basic mechanics test (tensile, compressive, and shear tests), are shown in Table 1.

Fig. 2 shows the flowchart of developed VUMAT subroutine for the 3D progressive damage simulation of composite materials. The FE simulation would be typically run from 0 to 6 ms, with 100 time-steps. Each computational time-step is performed for every appropriate single integration point. The numerical model continues to run till the defined total computation time had expired.

Table 1 Mechanical properties of composite laminates.

Properties	Values
Density（g/cm^3）	$\rho = 1.6$
Elastic properties（GPa）	$E_1 = 129$, $E_2 = E_3 = 9.83$, $G_{12} = G_{13} = 5.38$, $G_{23} = 3.42$
Poisson's ratio	$\upsilon_{12} = \upsilon_{13} = 0.31$, $\upsilon_{23} = 0.4$
Material strengths（MPa）	$X_T = 1733$, $X_C = 1264$, $Y_T = 68$, $Y_C = 225$, $S_{12} = 132$, $S_{13} = S_{23} = 112$
Critical fracture energy（mJ/mm^2）	$G_{ft}^c = 80$, $G_{fc}^c = 40$, $G_{mt}^c = 0.339$, $G_{mc}^c = 0.966$

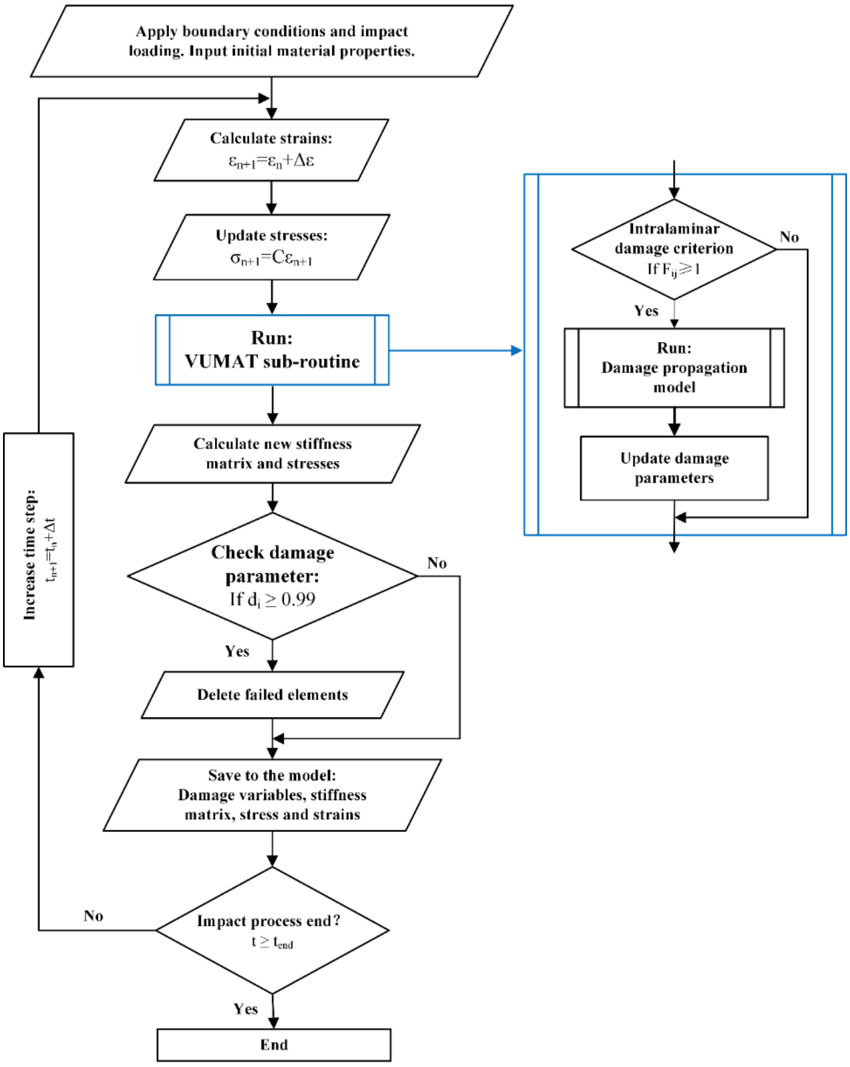

Fig. 2. The VUMAT subroutine flow chart of 3D progressive damage model for composites.

2.2 Interlaminar damage model

Delamination occurs in composite structures under impact loads due to local contact forces in critical regions. They are caused by the through-thickness shear and tensile properties, which are matrix-dominated and generally inferior compared to the in-plane properties.

In this paper, the employed interlaminar damage model is presented as an elastic constitutive relationship, which captures the response before the onset of delamination. The built-in cohesive elements in ABAQUS based on a bilinear traction-separation relationship are used to simulate the delamination failure at the interface between composite plies as shown in Fig. 3, in which the vertical axis refers to the traction and the two horizontal axes refer to the normal separation and the shear separation respectively. The intermediate vertical planes between two horizontal axes represents the damage responses under the mixed modes. The quadratic stress criterion is used to capture the initiation of delamination, given by:

$$\left(\frac{t_n}{N}\right)^2+\left(\frac{t_s}{S}\right)^2+\left(\frac{t_t}{T}\right)^2=1 \tag{23}$$

where, t_n、 t_s and t_t represent the normal and shear tractions; *N*, *S* and *T* denote the normal and shear interfacial strengths. When the expression of the quadratic stress criterion is satisfied, the interfacial damage initiates.

The Benzeggagh and Kenane (B-K) criterion [48], which is governed by mixed-mode fracture energy laws, is employed to govern the delamination propagation, given below:

$$G_C=G_{\mathrm{I}C}+\left(G_{\mathrm{II}C}-G_{\mathrm{I}C}\right)\left(\frac{G_{\mathrm{II}}}{G_{\mathrm{I}}+G_{\mathrm{II}}}\right)^{\eta} \tag{24}$$

where G_C, $G_{\mathrm{I}C}$ and $G_{\mathrm{II}C}$ are the total, normal (Mode I) and shear (Mode II) fracture energy, respectively. G_{I} and G_{II} are the Mode I and Mode II fracture energy release rate. η is the B-K exponent obtained by fitting the data obtianed from the mixed-mode bending tests. The interfaces between composite plies were modelled using the cohesive elements with the thickness defined as 0.01 mm. There are 19 interfaces between 20 composite plies, as shown in Fig. 4. The input parameters required for this element-based cohesive zone model have been given in Table 2.

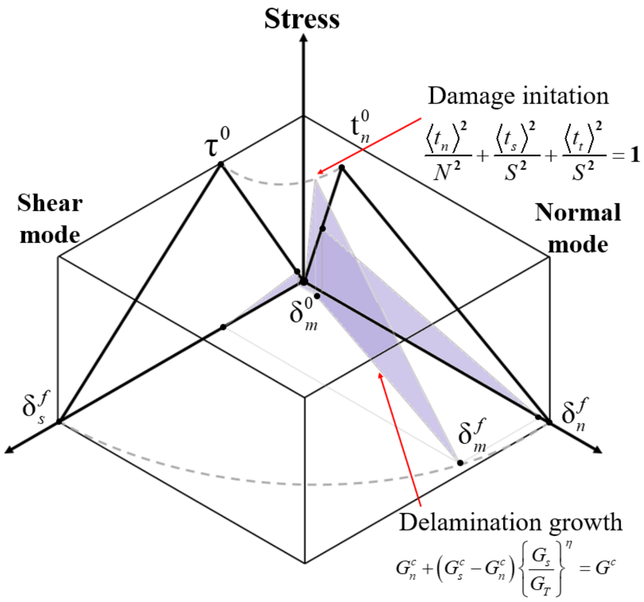

Fig. 3 Mixed-mode response for cohesive elements.

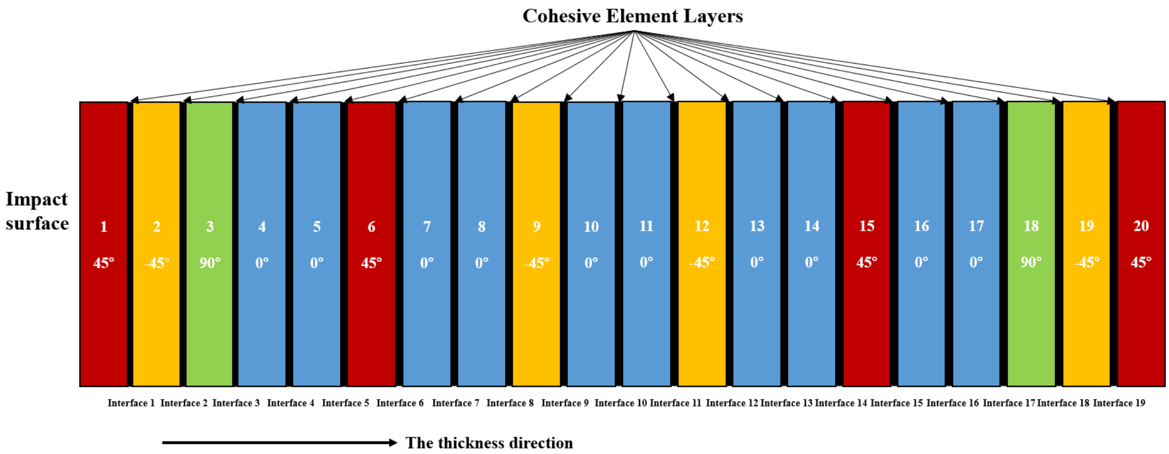

Fig. 4. The diagram of the cohesive element layers.

Table 2 Input parameters required for the cohesive zone model.

Properties	Values
Cohesive Strengths（MPa）	$t_n = 30$, $t_s = t_t = 30$
Initial cohesive stiffness（MPa/mm）	$K_{nn} = K_{ss} = K_{tt} = 1\times10^5$
Fracture Energy（J/mm^2）	$G_{IC} = 0.339$, $G_{IIC} = G_{IIIC} = 0.966$
Density（g/cm^3）	ρ=1.2
Benzeggagh-Kenane exponent	η=1.45

3 Finite element models

3.1 Low velocity impact modelling

The FE model is developed following the experimental set-up described in the ASTM D7136 standard. The mesh, geometry and boundary conditions of the simulation model are shown in Fig. 5. Four main features i.e. base fixture, composite laminates, clamps and impactor, are included to build up the assembly. Composite specimens have a layup of $[45/-45/90/0/0/45/0/0/-45/0]_s$ and a dimension of 150 mm×100 mm×5 mm. Each composite ply is meshed using eight-node linear hexahedral elements with reduced integration and hourglass control (C3D8R). In the composite specimens, a refined zone of 70×40 mm is created with an element size of 1 mm×1 mm and the remaining part is meshed using an element size of 2 mm×1 mm and 2 mm×2 mm to reduce the analysis time. As a result, the composite model proceeds an element number of 146,300 in total. The interfaces between the composite layers are modelled using eight-node 3D cohesive elements (COH3D8) with zero thickness. The zero thickness of cohesive elements here means the invisible thickness of the cohesive elements in visualisation. Theoretically, these zero thickness cohesive elements have a thickness of 0.01 for the numerical computation. The impactor is modelled as an analytical rigid body which is the spherical shape with a diameter of 16 mm. The reference lumped mass of the impactor is set as 7.05 kg. The 35 J impact energy is achieved by defining the initial velocity of the impactor as 3.14 m/s. The impact point is located in the centre of the composite laminates. In addition, both the base fixture with a centre cut-out of 125 mm × 75 mm and four clamps are modelled with discrete rigid bodies using hard contact interaction with the specimens.

The general contact is attributed to deal with the impactor/composite, the composite/base fixture and the clamps/composite contacts. The ‘hard’ contact relationship is adopted in the normal direction and the tangential behaviour use the friction formulation with a friction coefficient of 0.25. The total simulation period lasts 7 ms, and the stable incremental time is set to below 10^{-8} ms to achieve numerical convergence. Computations are completed using 16 CPUs on a Windows cluster with a running time of 30-60 h, depending on the number of the elements.

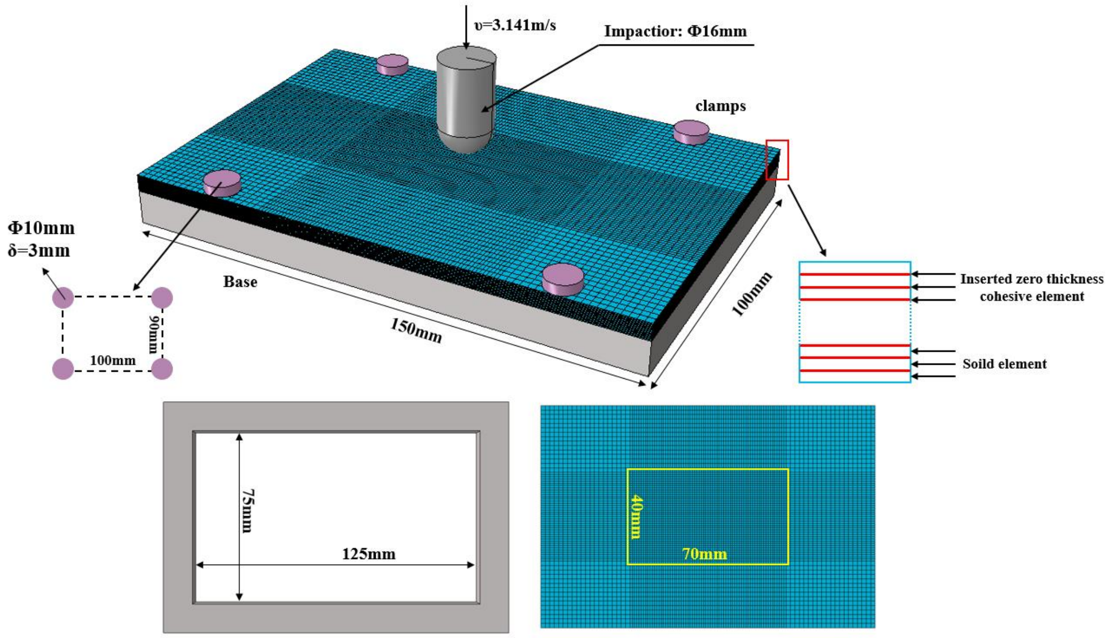

Fig. 5. The geometry and mesh of the FE model for the composite laminates on LVI.

3.2 Model of low velocity impact with pre-load

Based on the above FE model, a pre-load simulation is performed which follows two steps. Step-1 is defined first to introduce a pre-load into the model by applying pre-defined displacements or strains along the length of the specimen. The longitudinal micro-strains are applied to the two sides of the composite laminates in the 1 axis direction, as shown in Fig. 6. This is with an effective pre-tension or pre-compression load applied to generate a pre-strain with three magnitudes of 1000, 2000 and 3000 με. That is to say, before contact with the impactor, the samples have extensions of 0.15 mm, 0.3 mm and 0.45 mm respectively, along the lengthwise direction of the specimen. For the pre-tension and pre-compression, these are referred to as T1000/T2000/T3000 and C10000/C2000/C3000 respectively. During Step-1, an initial velocity of 3.14 m/s was pre-defined for the impactor but the impact process does not take place. Following the completion of Step-1, then, Step-2 begins and the impactor makes contact with the composite laminate with the pre-defined initial velocity of 3.14 m/s. The durations of Step-1 and Step-2 are set to 0.001 ms and 0.01 ms, respectively.

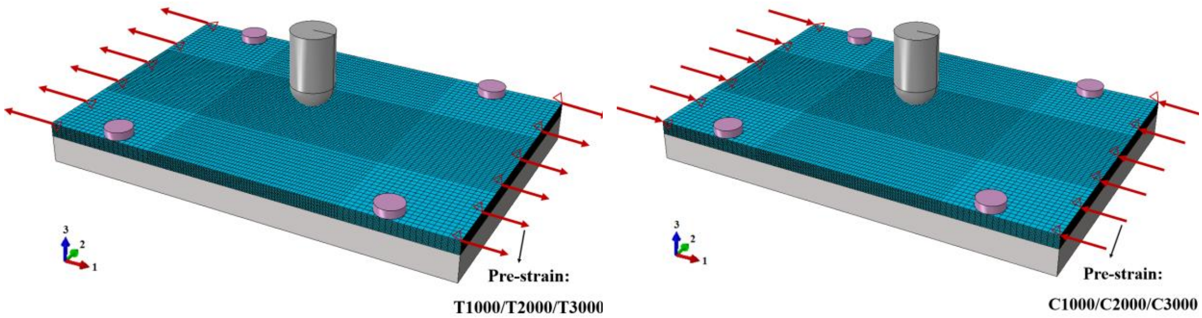

(a) (b)

Fig. 6. The boundary conditions for LVI on the composite laminates with the (a) Pre-tension (T1000/T2000/T3000) and (b) Pre-compression (C1000/C2000/C3000) loading conditions.

4 Model validation

For the validation of the model, low velocity impact experimental results for a CCF300/BA9916II carbon/epoxy composite were taken from the work performed by Zhang et al. [49]. There experimental tests reported in [ref] include three impact energy levels: 25 J, 35 J and 45 J. Ultrasonic C-scan inspections were performed to identify the delamination in the post-impacted specimens. Duplicate tests were performed to show a good consistency of measured experimental results. There is no obvious damage on the rear surface (non-impacted surface) of the samples tested at 25 J impact and the samples were seriously damaged subjected to 45 J impact. By contrast, the 35 J impact case has presented damage like fibre breakage and matrix cracking as well as delamination in an identifiable but not catastrophic extent. Therefore, in this research, the 35 J impact case has been selected to compare the results obtained from the experiment and simulation prediction.

As shown in Fig. 7, the load-time, load-displacement and energy-time curves obtained from the numerical prediction correlated with the corresponding experimental results reasonably well. A range of experimental data is shown with a grey shaded zone to demonstrate the variation. This is with specific experimental cases of blue, green and magenta solid lines. The dashed red line is the FE prediction and this lies well within the experimental tests. In particular, the FE prediction shows a drop in load followed by oscillations indicative of damage initiation at 8.6 kN and this is consistent with the experimental tests.

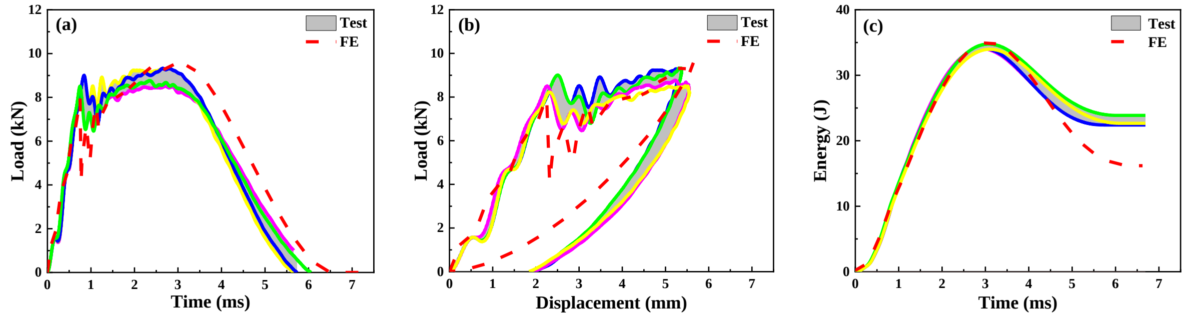

Fig. 7. Comparison of mechanical responses between LVI tests and simulation without pre-load for an impact velocity of 3.14 m/s (impact energy of 35 J): (a) load-time curve, (b) load-displacement curve and (c) energy-time curve (The grey shaded zone demonstrates variation in the experimental data. This is with specific experimental cases of blue, green and magenta solid lines. The dashed red line is the FE prediction.)

In the load-time and load-displacement curves, the initial increase in load is due to the elastic response of the specimens under impact loading. When the load increases monotonically up to a value of about 8.6 kN, a sharp drop of the load value is detected, indicating the onset of impact damage, which is mainly associated with matrix failure. Further load oscillations are successively observed due to damage propagation which may involve matrix cracking and delamination. Followed by an increase in load, the impactor reaches the maximum displacement and then is rebounded at this point, which is consistent with testing observations (Fig. 7b). Subsequently, the out-of-plane displacement of the laminate recovers gradually. The numerical load-time curve finds a good agreement with the experiment ones. The initial damage load, the maximum impact load and the impact duration are reproduced accurately (Fig. 7a). Regarding the energy-time curve (Fig. 7c), when the impactor contacts with the composite laminates, the kinetic energy of impactor starts to be transformed to the energy of the composite laminates, which includes the stored elastic energy and the damage dissipated energy. When the impact velocity is zero, the loss of kinetic energy of the impactor reaches the maximum value, then the elastic energy stored in the composite panel drives the recovery of panel to rebound the impactor, which results in the decrease in the energy-time curves. The finally achieved stable value indicates the energy dissipated during the impact event. The overall energy-time history predicted by the numerical model presents a generally good agreement with the experimental ones.

Fig. 8 exhibits the comparison between the experimental and numerical results. The matrix damage can be observed on the rear surface of composite laminates after LVI experiments, as shown in Fig. 8a. The matrix cracking tends to distribute along the 45 degree in the bottom lamina. Fig. 8b shows the FE numerically predicted matrix damage (red zone) on the back surface of the laminates. Due to the smeared-crack and homogenised natures of the employed model, the 45 degree long cracks between the fibre bundles were not completely captured, while the overall matrix damage on the rear surface of the post-impacted samples have been reasonably captured. This demonstrates that the employed meso-scale smeared-crack model is able to capture the location and propagation of damage in the composite samples due to impact.

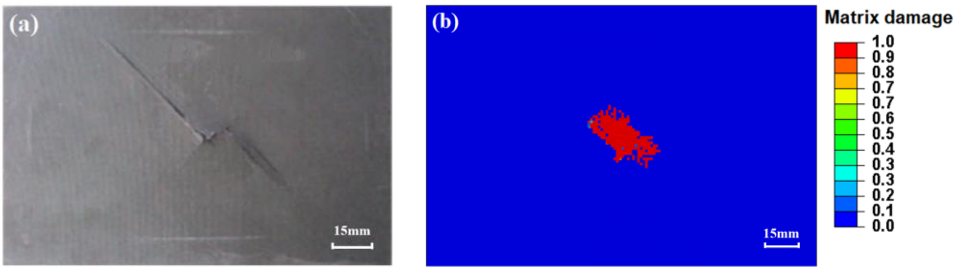

Fig. 8. Damage on the back surface of composite laminates of LVI test and simulation for an impact velocity of 3.14 m/s (impact energy of 35 J): (a) experimental damage and (b) FE predicted damage.

A comparison between the experimentally measured and the numerically predicted delamination damage footprint obtained from the composite specimens under LVI has been made as shown in Fig. 9. The dark blue represents the C-scan reflection from the bottom (non-impacted) surface of the composite laminates and the dark red refers to the C-scan reflection from the top (impacted) surface. For the convenience of comparison, the footprint of the numerically predicted delamination area has been presented as the white dash line. The 0° arrow indicates the longitudinal direction. The area of each delamination map was calculated by counting the total numbers of pixels and dark-blue pixels, which represent the total area of the sample and the non-damaged area after impact respectively, using an in-house MATLAB script. According to the calculated total pixels and dark-blue pixels, the number of the remaining pixels, which refers to the damage area, can be subsequently determined. The experimentally obtained delamination area is 964 mm^2, and the simulated delamination area is 740 mm^2, which is ca. 23% deviation from the experimental delamination area which is reasonable.

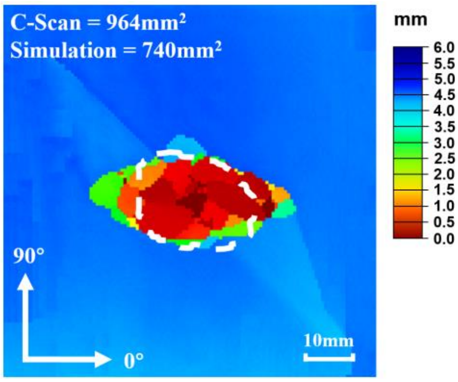

Fig. 9 Comparison of damage footprints obtained from the LVI test (cloud maps) and simulation (white dash line) for an 35 J impact case.

To summarise, Table 3 has been presented to show the comparison between the numerical and experimental results, regarding the maximum load, the impact duration time, the maximum displacement, the absorbed energy and delamination area. Deviations between experimental and numerical values are in a reasonable range, from ca. 5% to ca. 28%, showing a generally good agreement between the experimental and numerical results.

Mesh size is considerably important for the computational convergence and simulation efficiency. In this paper, the selection of the mesh size was made based on the results obtained from the simulations with three different mesh sizes (Size - 0.5, equivalent to 0.5 × 0.5 mm; Size – 1, equivalent to 1 × 1 mm and Size – 2, equivalent to 2 × 2 mm mesh size). Fig. 10 presents the load-time and load-displacement curves obtained from the simulations with these three different mesh sizes. The results show that when the mesh size is 0.5 × 0.5 mm (Size - 0.5) and 1 × 1 mm (Size – 1), the predicted load response best is similar and correlates reasonably well with the experimental (Test) results.

Table 3 Comparison of main data between LVI tests and simulation without pre-load.

	Maximum load (kN)	Impact duration (ms)	Maximum displacement (mm)	Absorbed energy (J)	Delaminated area (mm^2)
Test	9.0	5.9	5.4	22.4	964
FE	9.6	6.6	5.7	16.2	740
Deviation	6.7%	11.8%	5.6%	27.6%	23.2%

The maximum load, the maximum displacement and the computational time are compared in Fig. 11. The simulation with 1 × 1 mm mesh size (Size 1) delivers the best agreement on the overall response of all three simulation cases. As a result, the mesh size of the central region 1 mm × 1 mm (Size – 1) for the composite laminates was selected for all future simulations. This is deemed to be able to achieve a good balance between the computational accuracy and efficiency.

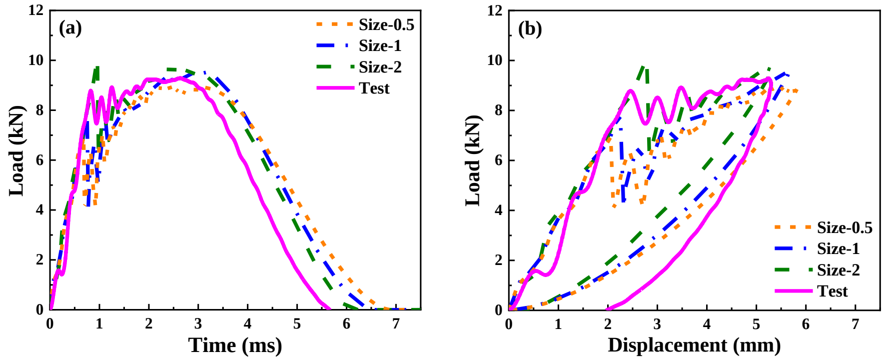

Fig. 10. Comparison of mechanical response between LVI test and simulations with different mesh sizes (Size - 0.5, equivalent to 0.5 × 0.5 mm; Size-1, equivalent to 1 x 1 mm and Size-2, equivalent to 2 × 2 mm mesh size) for an impact velocity of 3.14 m/s (impact energy of 35 J): (a) load-time curve and (b) load-displacement curve.

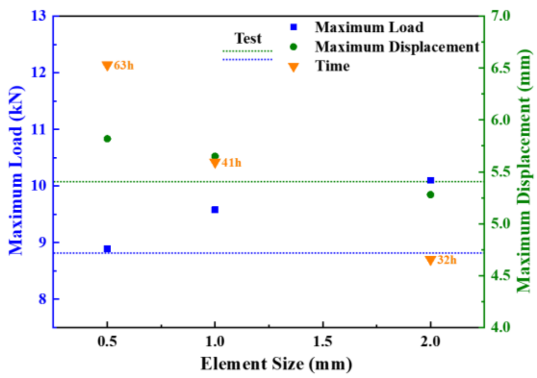

Fig. 11. Mesh-sensitivity on LVI composite tests and simulation results for an impact velocity of 3.14 m/s (impact energy of 35 J).

5 Effects of pre-load on impact response

5.1 Model set-up

For the simulations to be performed, an effective pre-tension or pre-compression load was applied to generate a pre-strain with three magnitudes of 1000, 2000 and 3000 με along the length of the specimen. It was found better to define the initial pre-strain along the length of the specimen and these are given in Table 4.

Table 4 Types and magnitudes of pre-loads applied to the composite laminates.

Degree of pre-loads	**Codes**	**Pre-strain magnitudes（με）**
No pre-load	Non-preloaded	0
Pre-tension	T1000	1000
	T2000	2000
	T3000	3000
Pre-compression	C1000	1000
	C2000	2000
	C3000	3000

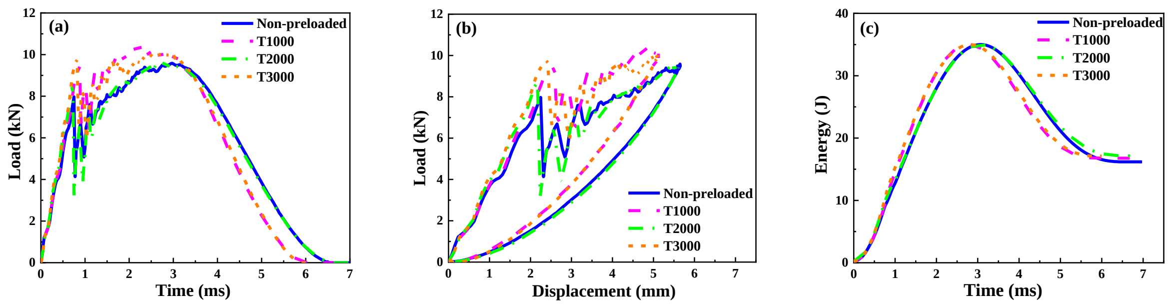

Fig. 12. Mechanical response of LVI, under different pre-tension loads, to give initial 1000, 2000 and 3000 με (along length of specimen) for an impact velocity of 3.14 m/s (impact energy of 35 J): (a) load-time curve, (b) load-displacement curve and (c) energy-time curve.

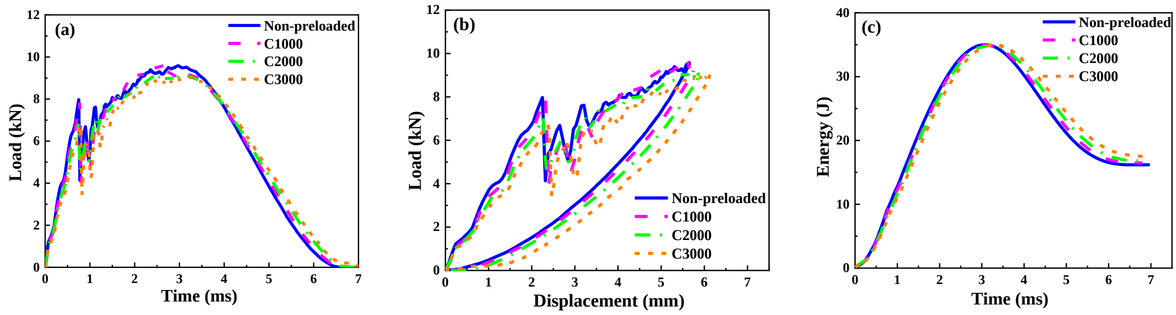

Fig. 13. Mechanical response of LVI, under different pre-compression loads, to give initial 1000, 2000 and 3000 με (along length of specimen) for an impact velocity of 3.14 m/s (impact energy of 35 J): (a) load-time curve, (b) load-displacement curve and (c) energy-time curve.

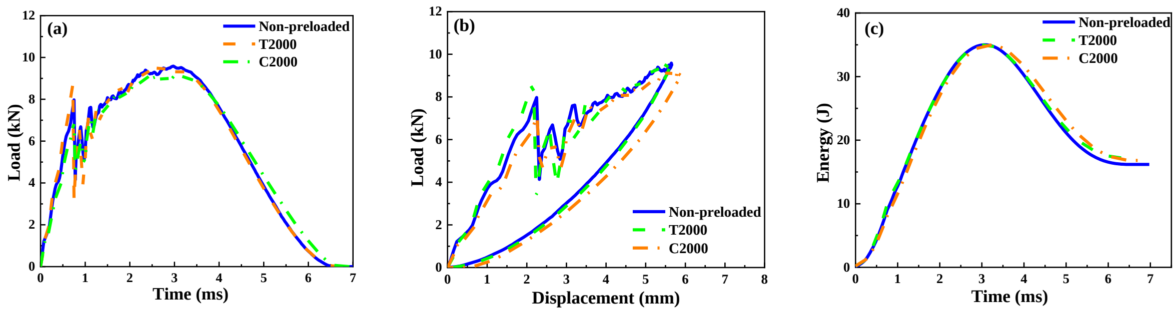

Fig. 14. Mechanical response of LVI, under pre-tension and pre-compression, to give tensile and compressive micro-strain of 2000 με (along length of specimen) compared with no pre-load, for an impact velocity of 3.14 m/s (impact energy of 35 J): (a) load-time curve, (b) load-displacement curve and (c) energy-time curve.

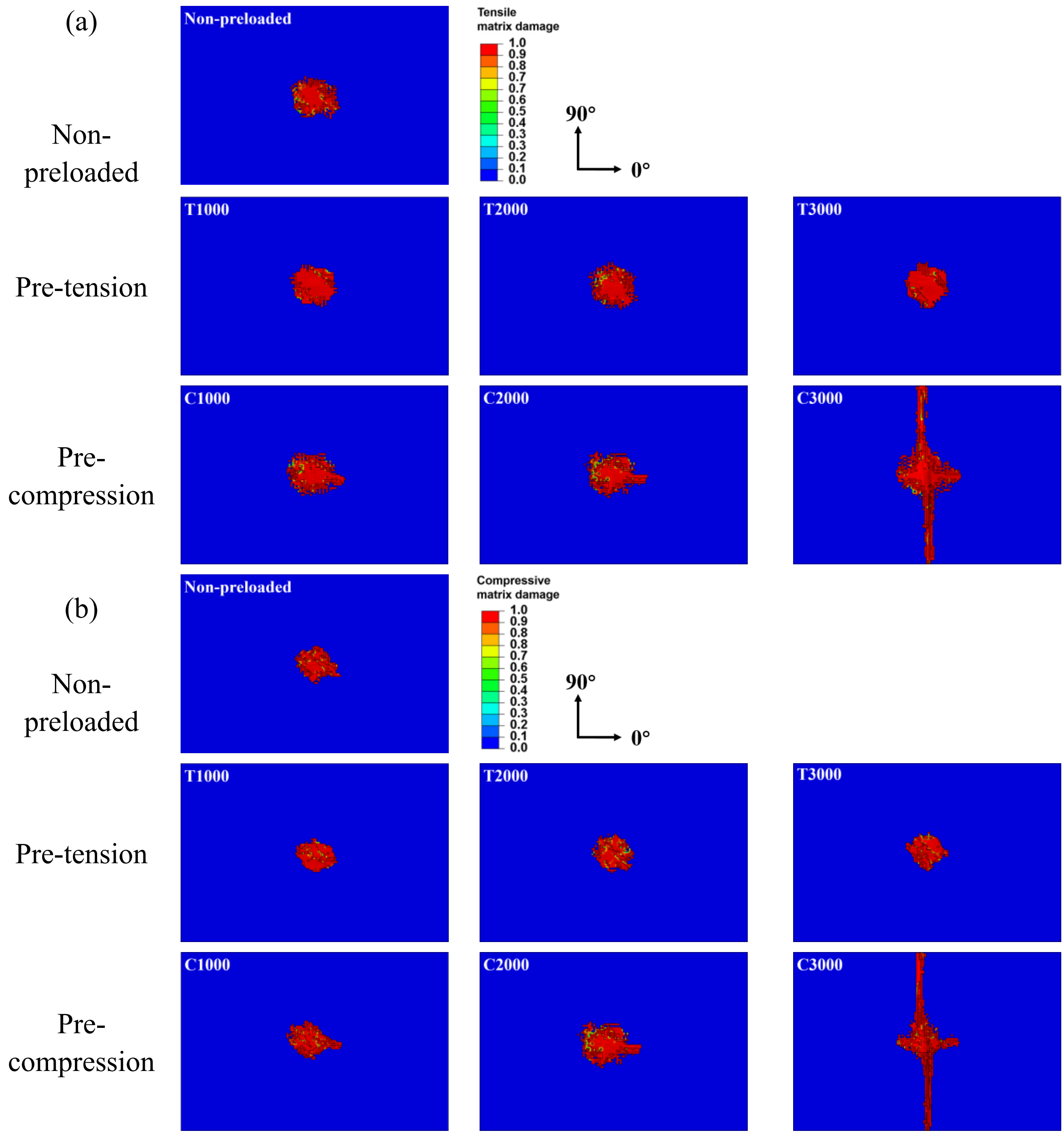

Fig. 15. Matrix damage obtained from simulations with different pre-loads (to give tensile and compressive pre-strains 1000, 2000 and 3000 με) for an impact velocity of 3.14 m/s (impact energy of 35 J): (a) tensile matrix damage and (b) compressive matrix damage.

5.2 Pre-load effects on overall response

Load-time, load-displacement and energy-time relations of impacts, for an impact velocity of 3.14 m/s (impact energy of 35 J), were simulated for different compressive and tensile pre-loads and these results are shown in Fig. 12 and 13. It is found that the pre-loads, and associated pre-strains, have a significant influence on the impact behaviour of composite laminates.

Compared to non-preloaded condition, pre-tension load gives rise to a ‘stiffening’ effect on the laminates, which can be seen from the slope of the load-displacement curve as shown in Fig. 12b. The higher the pre-tension load, the higher the slope, that is the stiffer response of the composite laminates. Load-time curves show a time scaling effect with the pre-tension loads, where the impact event becomes shorter for pre-tension load increasing. Moreover, peak load increases and maximum displacement decreases with increase in tensile pre-load (Figs.12a and 12b), in agreement with [50]. On the other hand, these trends are opposite in effect under the pre-compression load, which softens the load response of the composite laminates as shown in Figs.13a and 13b.

The energy-time curves are plotted in Figs. 12c and13c. An initial rise occurs as kinetic energy is converted into strain energy with some losses due to damage, damping and other processes. The stored strain energy then rebounds the impactor. It is to be noted that the presence of pre-compression loads leads to slightly more energy being absorbed by the laminates, indicative of more damage under pre-compression loads.

The possible reason is that the pre-tension load stiffens the response of the composite laminates, which can lead to a smaller displacement and higher impact load. On the other hand, the pre-compression load softens the response of composite laminates with the laminates exhibiting more out-of-plane deformation. Moreover, these influences are enhanced by increasing the magnitude of pre-loads.

For comparison, Fig. 14 plots the impact response curves of pre-tension and pre-compression loads with the same pre-applied micro-strain of 2000 με. This shows clearly the pre-tension and pre-compression loads have converse effects on the loading responses of composite laminates.

5.3 Pre-load effects on matrix damage

Fig. 15 presents a comparison of the predicted intralaminar (matrix cracking) damage for pre-tension and pre-compression, with different pre-loads, subjected to LVI. These data are compared with the non-pre-loaded case. Both tensile matrix damage and compressive matrix damage are presented. It can be seen that pre-loads are applied giving pre-strains of 1000, 2000 and 3000 με. These cases are labelled T1000, T2000 and T3000 for tensile pre-load and C1000, C2000 and C3000 for the compressive pre-load. There are distinct differences in damage behaviour for the pre-tension and pre-compression cases. Pre-tension load has very little effect on the extent of matrix damage, albeit tensile matrix damage slightly more than the compressive matrix damage in all cases. However, the pre-compression affects appreciably the matrix damage. Overall, the longitudinal extent, or dimension, of the matrix damage area (shown as the red zone in Fig. 15) are similar for T1000, T2000 and T3000 cases. However, for the compressive pre-loads, the longitudinal extent, or dimension, of the matrix damage area increases by ca. 20%, 30% and 45% respectively for C1000, C2000 and C3000 cases. There is less influence of pre-compression on the width of the matrix damage, except for the special case C3000, in which the pre-compression has extensively increased the width-wise dimension of the impact matrix damage. This full width-wise damage occurs during the simulation of the impact event and is not due to the initial compressive pre-loading of the laminate.

In order to further evaluate the effects of pre-load on matrix damage, Fig. 16 presents the changes in tensile and compressive matrix damage with increasing pre-load. It can be seen that tensile and compression matrix damage areas increase with pre-compression load (pre-strain) and this is particularly obvious for the 3000 micro-strain case in which the tensile damage area increases significantly. The pre-tension load causes very little change in matrix damage area. This may be because the matrix damage laminates is dominated by impact load under relatively low level pre-tension load, and the effect of pre-tension load is not reflected [50]. In contrast, a continuous and obvious positive effect on the matrix damage have been observed for the pre-compression load, which indicates that damage in the composite laminates is in the pre-load dominated mode [50].

To figure out the transition from impact-dominated to pre-load dominated mode, five more pre-load cases, T500, T4000, T5000 and C500, C4000, have been added to the simulation. The overall matrix damage, including both the tensile and compressive damage, obtained from these five additional pre-load cases are compared with those obtained from other exiting pre-load cases, as shown in Fig. 17. It can be seen that when the pre-tension load is between T500 and T3000, the overall matrix damage area is almost consistent, while when the pre-load increased from T3000 to T5000, the overall matrix damage experienced a significant growth. For the pre-compression cases, when the pre-loads are C500 and C1000, no obvious change was observed from the overall matrix damage, while when the pre-compression load is between C1000 and C4000, abrupt growth was found in the overall matrix damage. Based on these observations, we can determine that, for the pre-tension and pre-compression cases, the responses of composite laminates transformed from impact-dominated mode to pre-load dominated mode at T3000 and C1000, respectively.

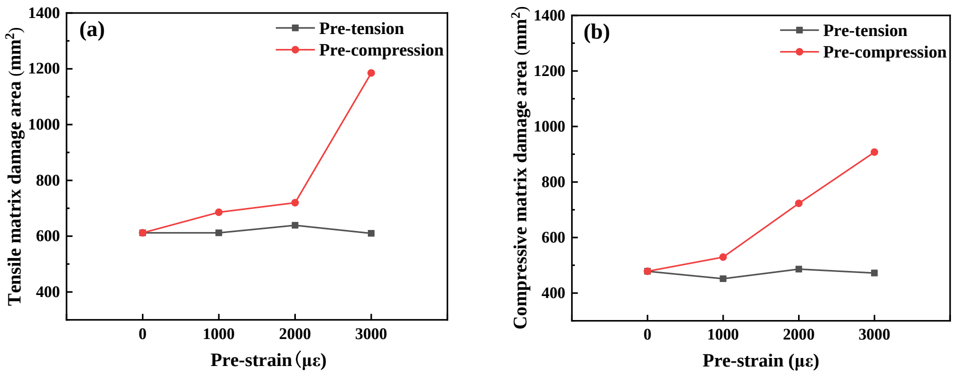

Fig. 16. Matrix damage areas obtained from the LVI simulations with no pre-load and different pre-loads (to give compressive and tensile pre-strains 1000, 2000 and 3000 με) for an impact velocity of 3.14 m/s (impact energy of 35 J):(a) tensile matrix damage areas and (b) compressive matrix damage areas.

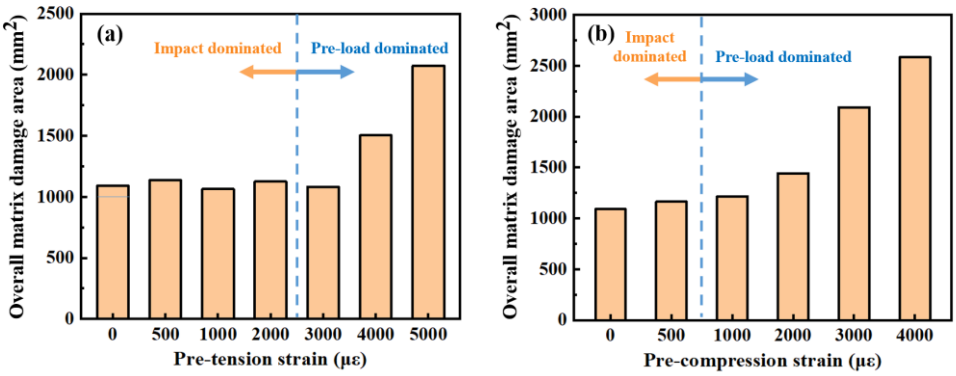

Fig. 17 The relationship between the overall matrix damage areas and the magnitudes of pre-loads: (a) pre-tension strain and (b) pre-compression strain.

5.4 Effects of pre-load on delamination

Fig. 18 shows the predicted delamination footprints, for an impact velocity of 3.14 m/s (impact energy of 35 J) on non-preloaded, pre-tension and pre-compression laminates. An approximately circular delamination footprint has been observed for the non-preloaded case. For the composite laminates with the pre-tension loads, the delamination footprint is circular in shape and of slightly reduced size with the length and width of the damaged area decreasing slightly by 5-10%. For composite laminates with pre-compression loads, the shapes of the delamination footprint becomes elliptic in shape with the major axis aligned with the longitudinal direction of the composite laminate. This is thought to be due to the increasing delamination near the back surface of the specimen. By comparing the length and width of the damage contours in Fig. 18 (for pre-tension and pre-compression cases), it is found that the pre-compression load increases the length and width of the delamination footprint by up to ca. 25%.

Compared to other laminates, much more serious damage has been observed from the composite laminates subjected to C3000 pre-load which corresponds to a compressive pre-strain of 3000 με. To derive insight into this phenomenon, the matrix damage in composite laminates under C3000 pre-load after LVI event has been extracted and shown in Fig. 19. It was found that no damage occurred in the composite laminates after applying this C3000 pre-compression load. However, when the panel undergoes deformation during impact, matrix damage and delamination propagate extensively along the width or transverse direction of the composite laminate. This abrupt increase in measured areas regarding matrix damage might be related to the occurrence of buckling during failure process, which can enhance the pre-load effects on the matrix damage in composite laminates.

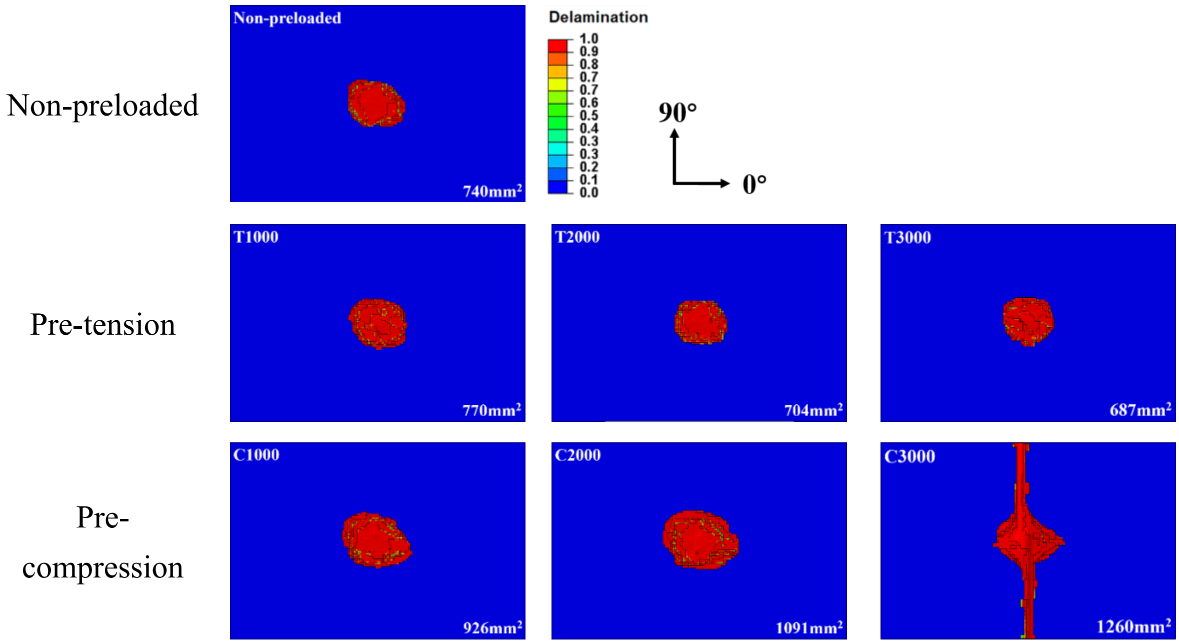

Fig. 18. LVI induced delamination footprints in the composite laminates with different pre-loads (to give compressive and tensile pre-strains of 1000, 2000 and 3000 με).

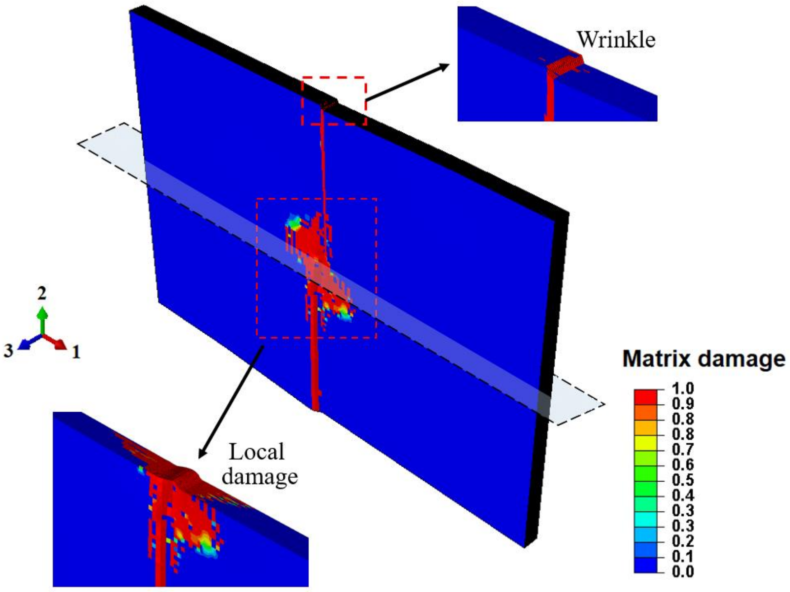

Fig. 19. Matrix damage obtained from LVI simulation with C3000 pre-compression load.

As shown in Fig. 20, the delamination of composite laminates is significantly affected when pre-compressions of 1000, 2000, and 3000 με are applied and increases linearly with pre-compression strain. For the pre-tension case, the delamination area fluctuates but overall decreases slightly with pre-tension strain. For the pre-compression load case, the increase in delamination area is related to the increase in intralaminar (matrix) damage observed. For the pre-tension load case, Mikkor et al [51] have suggested that there is a stiffening or inhibiting effect with the pre-tension load preventing bending deflections of laminates that typically facilitate delamination.

Fig. 21 plots the damage areas of each cohesive interface obtained from the composite laminates subjected to T2000 pre-tension, non-preloaded and C2000 pre-compression cases at an impact velocity of 3.14 m/s (impact energy of 35 J). The results show that damage areas of the cohesive interfaces are suppressed by pre-tension load, especially for interface 10 and interface 19. The pre-compression load aggravates the cohesive damage (delamination), especially for the interfaces 8, 9, 11 and 12. These phenomena can be explained by pre-tension slightly inhibiting delamination. There is a reinforcing effect from pre-compression on the out-of-plane deformation of composite plies, which can directly affect the delamination propagation in the composite laminates under impact loading. The pre-tension can suppress the out-of-plane deformation whilst the pre-compression can exacerbate the out-of-plane deformation. Moreover, it is found that the degree of influence of pre-load on the cohesive damage is related to the lay-up angle of the adjacent composite plies.

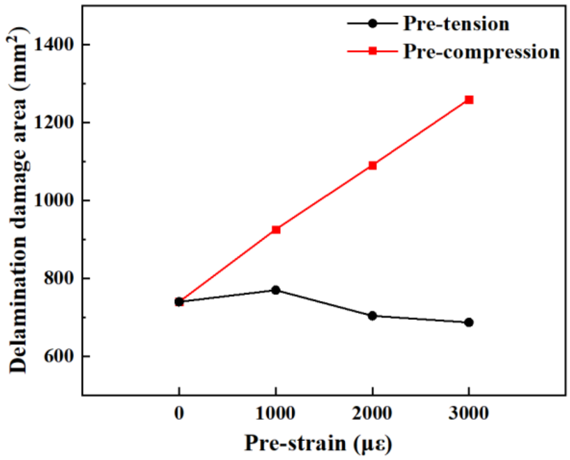

Fig. 20. Delamination damage area under LVI for different pre-strains at an impact velocity of 3.14 m/s (impact energy of 35 J).

The extent of cohesive zone failure, or delamination, at each of the cohesive interfaces 9 (-45/0), 10 (0/0) and 11 (0/-45) when subjected to the different pre-loads (T1000 to T3000 and C1000 to C3000) and non-preloaded cases, are presented in Fig. 22. This is for an impact velocity of 3.14 m/s (impact energy of 35 J). Under pre-tension load, the damage areas, at the cohesive interfaces 9, 10 and 11, are similar or decrease slightly with the pre-tension load. However, the damage areas, at the cohesive interfaces 9, 10 and 11, increase slightly with the pre-compression load. It is thought that pre-compression load makes the composite plies with the lay-up angles -45° and 0° more prone to a large bending during the impact process. This is with the consequence that interfaces of laminae with the -45° and 0° lay-up angles show greater propensity for delamination. When plies are subjected to pre-tension load along the longitudinal direction, the cohesive damage at the interface is inhibited slightly due to the reduced bending.

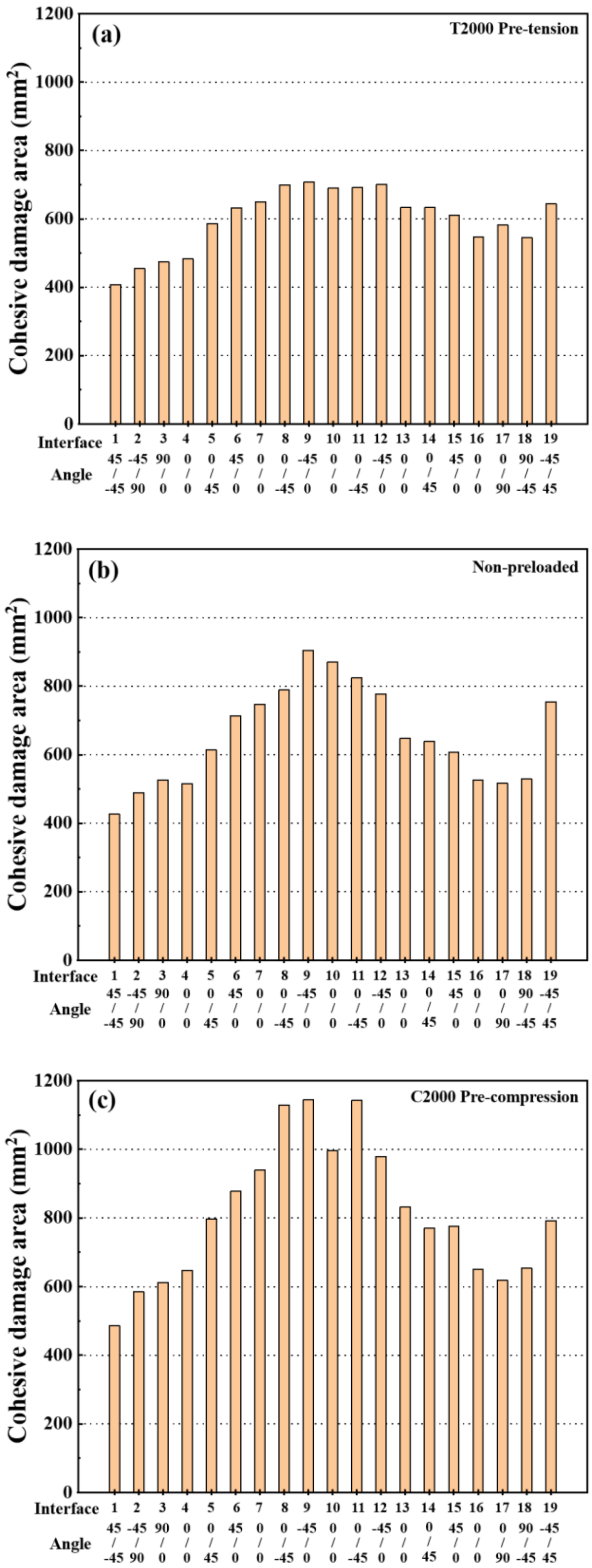

Fig. 21. Cohesive damage areas obtained from each composite laminate interface at an impact velocity of 3.14 m/s (impact energy of 35 J) for: (a) pre-tension (T2000), (b) non-preloaded, (c) pre-compression (C2000).

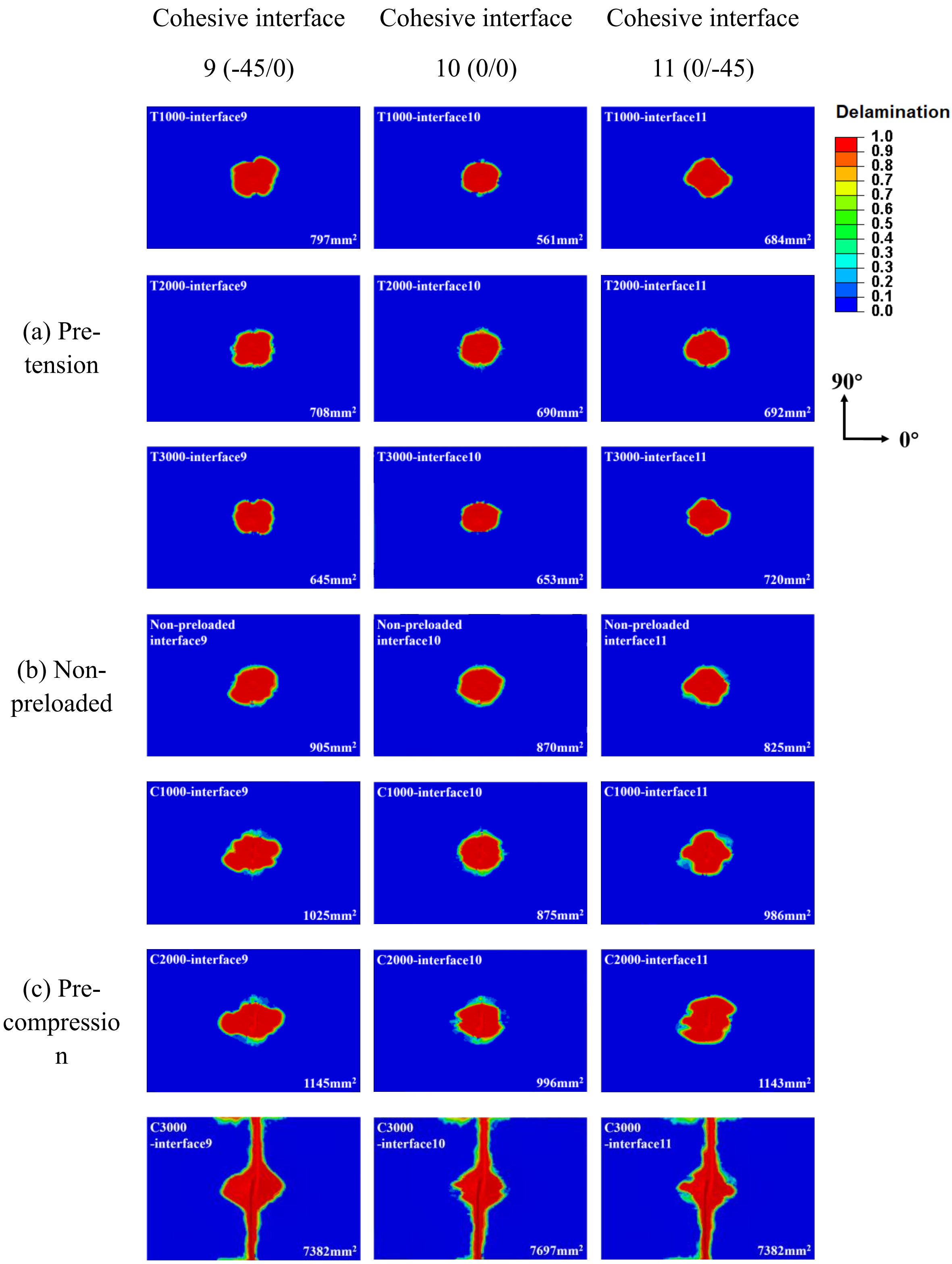

Fig. 22. Predicted delamination on the cohesive interfaces 9, 10 and 11 at an impact velocity of 3.14 m/s (impact energy of 35 J) for: (a) pre-tension, (b) non-preloaded and (c) pre-compression.

6 Conclusions

The effects of pre-load on the low velocity impact response of composite laminates under different conditions of pre-loads have been investigated. A three-dimensional progressive damage model has been established, implementing a VUMAT subroutine using the finite element package ABAQUS/Explicit. The composite damage model is validated against experimental results. This validated model is then employed to predict the impact behaviour of composite laminates with different types of pre-load. It has been shown that pre-load has appreciable influence on the loading response of composite laminates. This is with pre-tension load tending to 'stiffen' the response of composite laminates, whilst pre-compression load tends to 'soften' the response of the composite laminates. It is also observed that the presence of pre-compression load has caused more damage in composite laminates under impact. When the pre-compression strain increases to 3000 με, the impact damage extended across the width of the composite laminate.

It has been shown that pre-load influences the area and shape of the delamination footprint during low-velocity impact. The delamination area footprint increases noticeably due to pre-compression load and decreases slightly under the pre-tension load. It has also been shown that the degree of influence of pre-load on the cohesive damage is related to the lay-up angle of the adjacent composite plies. These effects have been observed by other researchers. For example, the impact response of pre-load was in reasonable agree with the earlier experimental tests conducted by Heimbs et al. [16] and Zhikharev et al. [50]. Similar effects have also been observed by Hu et al. [26] who showed that pre-tension load plays a strengthening role in the composite laminates whereas pre-compression load has the opposite effect.

It is deemed that the developed computational model is able to effectively serve as a numerical tool to provide guidance to the design and maintenance of composite structures exposed to pre-load conditions and impact threats.

CRediT authorship contribution statement

Wenxin Zhang: Investigation, Methodology, Formal analysis, Data curation, Writing- original draft. **Di Zhang**: Methodology, Formal analysis. **Jin Zhou**: Conceptualization, Methodology, Resources. **Jiangwei Qi**: Methodology, Data curation. **Wen Zhao**: Investigation, Formal analysis. **Shuming Yang**: Writing review & editing. **John P. Dear**: Writing, review & editing. **Haibao Liu**: Writing, review & editing.

Declaration of competing interest

The authors declare that they have no known competing financial interests or personal relationships that could have appeared to influence the work reported in this paper

Acknowledgements

This study was supported by the National Natural Science Foundation of China (Grant numbers. 12002265) and China Postdoctoral Science Foundation (Program numbers. 2021M962572).

References

[1] A. Vlot, M. Krull, Impact damage resistance of various fibre metal laminates, J Phys Iv 7 (1997) 1045−1050, doi:10.1051/jp4:19973176.

[2] S. Boria, A. Scattina, G. Belingardi, Impact behavior of a fully thermoplastic composite, Compos Struct. 167 (2017) 63−75, doi:10.1016/j.compstruct.2017.01.083.

[3] A. Arjangpay, A. Darvizeh, M. Yarmohammad. Tooski, R. Ansari, An experimental and numerical investigation on low velocity impact response of a composite structure inspired by dragonfly wing configuration, Compos Struct. 184 (2018) 327−336, doi:10.1016/j.compstruct.2017.10.006.

[4] SZH. Shah, PSM. Megat-Yusoff, S. Karuppanan, RS. Choudhry, F. Ahmad, et al., Performance comparison of resin-infused thermoplastic and thermoset 3D fabric composites under impact loading, Int. J. Mech. Sci. 189 (2021) 105984, doi:10.1016/j.ijmecsci.2020.105984.

[5] N. Alzeanidi, H. Ghasemnejad, Analysis of the effect of impact damage on the repairability of composite panels, Compos. Struct. 176 (2017) 304–312, doi:10.1016/j.compstruct.2017.05.054.

[6] HJ. Zhang, YY. Ge, H. Tang, YY. Shi, YG. Miao, Y. Hu, Examination of low-velocity impact and mechanical properties after impact of fiber-reinforced prepreg composites, Polym. Compos.

40 (2019) 2154–2164, doi:10.1002/pc.25002.

[7] KX. Lin, M. Zeng, HM. Chen, XM. Tao, YF. Ouyang, et al., Dynamic strength, reinforcing mechanism and damage of ceramic metal composites, Int. J. Mech. Sci. 231 (2022) 107580, doi:10.1016/j.ijmecsci.2022.107580.

[8] L. Xiao, GH. Wang, S. Qiu, ZX. Han, XD. Li, DX. Zhang, Exploration of energy absorption and viscoelastic behavior of CFRPs subjected to low velocity impact, Composites B 165 (2019) 247–254, doi:10.1016/j.compositesb.2018.11.126.

[9] HB. Liu, BG. Falzon, JP. Dear, An experimental and numerical study on the crush behaviour of hybrid unidirectional/woven carbon-fibre reinforced composite laminates, Int. J. Mech. Sci. 164 (2019) 105160, doi:10.1016/j.ijmecsci.2019.105160.

[10] LR. Xu, A. Karakoç, M. Flores, HB. Ning, E. Taciroglu, Predicting the upper-bound of interlaminar impact damage in structural composites through a combined nanoindentation and computational mechanics technique, Compos. Struct. 286 (2022) 115110, doi:10.1016/j.compostruct.2021.115110.

[11] OH. Hassoon, M. Tarfaoui, A. El Malki Alaoui, A.El. Moumen, Mechanical behavior of composite structures subjected to constant slamming impact velocity: An experimental and numerical investigation, Int. J. Mech. Sci. 144 (2018) 618–627, doi:10.1016/j.ijmecsci.2018.05.035.

[12] HB. Liu, J. Liu, YZ. Ding, ZE. Hall, XS. Kong, J. Zhou, et al., A three-dimensional elastic–plastic damage model for predicting the impact behaviour of fibre-reinforced polymer–matrix composites, Composites B 201 (2020) 108389, doi:10.1016/j.compositesb.2020.108389.

[13] SC. Long, XH. Yao, HR. Wang, XQ. Zhang, A dynamic constitutive model for fiber-reinforced composite under impact loading, Int. J. Mech. Sci. 166 (2020) 105226, doi:10.1016/j.ijmecsci.2019.105226.

[14] B. Whittingham, IH. Marshall, T. Mitrevski, R. Jones, The response of composite structures with prestress subject to low velocity impact damage, Compos. Struct. 66 (2004) 685–698,doi:10.1016/j.compstruct.2004.06.015.

[15] SK. García-Castillo, S. Sánchez-Sáez, J. López-Puente, E. Barbero, C. Navarro, Impact behaviour of preloaded glass/polyester woven plates, Compos. Sci. Technol. 69 (2009) 711–717, doi:10.1016/j.compscitech.2008.01.007.

[16] S. Heimbs, S. Heller, P. Middendorf, F. Hähnel, J. Weiße, Low velocity impact on CFRP plates with compressive preload: Test and modelling, Int. J. Impact. Eng. 36 (2009) 1182–1193, doi:10.1016/j.ijimpeng.2009.04.006.

[17] H. Saghafi, G. Minak, A. Zucchelli, Effect of preload on the impact response of curved composite panels, Composites B 60 (2014) 74–81, doi:10.1016/j.compositesb.2013.12.026.

[18] NASA Workshop on Impact Damage to Composites, NASA conference publication, Hampton VA, 1991.

[19] AT. Nettles, DG. Lance, The Effect of Compressive Preload on the Compression-After-

Impact Strength of Carbon/Epoxy, NASA technical paper TP3303, 1992.

[20] S. Heimbs, T. Bergmann, D. Schueler, N. Toso-Pentecôte, High velocity impact on preloaded composite plates, Compos. Struct. 111 (2014) 158–168, doi:10.1016/j.compstruct.2013.12.031.

[21] FAA Advisory Circular, 107B Composite Aircraft Structures: AC20-107B, Federal Aviation Administration, Washington, D. C., 2009.

[22] JQ. Hu, CM. Ji, S. Chen, S. Li, YJ. Zou, Two-position impact behavior and interference mechanism of CFF/PEEK thermoplastic composites, Int. J. Mech. Sci. 232 (2022) 107644, doi:10.1016/j.ijmecsci.2022.107644.

[23] SY. Li, WY. Liu, YQ. Mao, SJ. Hou, Numerical cross-scale optimization of homogenized composite laminates under impact loading, Int. J. Mech. Sci. 245 (2023) 108108, doi:10.1016/j.ijmecsci.2023.108108.

[24] BB. Liao, JW. Zhou, Y. Li, PD. Wang, X. Li, Damage accumulation mechanism of composite laminates subjected to repeated low velocity impacts, Int. J. Mech. Sci. 182 (2020) 105783, doi:10.1016/j.ijmecsci.2020.105783.

[25] N. Guillaud, C. Froustey, F. Dau, P. Viot, Impact response of thick composite plates under uniaxial tensile preloading, Compos. Struct. 121 (2015) 172–181, doi:10.1016/j.compstruct.2014.11.021.

[26] Y. Hu, DS. Liu, J. Guo, YY. Shi, CW. Shan, Low-velocity impact damage research on 2-dimentional UHMWPE/CF hybrid woven laminates under preloading, Thin-Walled Struct. 161 (2021) 107472, doi:10.1016/j.tws.2021.107472.

[27] Y. Hu, YY. Shi, DS. Liu, JF. Zhang, Low-velocity impact damage tolerance of ultrahigh molecular weight polyethylene/carbon fiber laminates under prestress, Polym. Compos. 43 (2022) 712–729, doi:10.1002/pc.26404.

[28] Y. Hu, YY. Shi, DS. Liu, J. Guo, JF. Zhang, et al., Damage tolerance of 2-dimentional UHMWPE/CF hybrid woven laminates subjected to low-velocity impact, Mater. Des. 191 (2020) 108604, doi:10.1016/j.matdes.2020.108604.

[29] SMR. Khalili, RK. Mittal, NM. Panah, Analysis of fiber reinforced composite plates subjected to transverse impact in the presence of initial stresses, Compos. Struct. 77 (2007) 263–268, doi:10.1016/j.compstruct.2005.08.027.

[30] IH. Choi, Low-velocity impact analysis of composite laminates under initial in-plane load, Compos. Struct. 86 (2008) 251–257, doi:10.1016/j.compstruct.2008.03.042.

[31] A. Kurşun, M. Şenel, HM. Enginsoy, Experimental and numerical analysis of low velocity impact on a preloaded composite plate, Adv. Eng. Softw. 90 (2015) 41–52, doi:10.1016/j.advengsoft.2015.06.010.

[32] F. Ruivo Fuga, MV. Donadon, Low velocity impact on pre-loaded composite plates: A novel standard-based experimental apparatus, Compos. Struct. 261 (2021) 113315, doi:10.1016/j.compstruct.2020.113315.

[33] M. Rathnasabapathy, AP. Mouritz, AC. Orifici, Impact-under-load damage tolerance of a fibre metal laminate, Compos. Struct. 287 (2022) 115368, doi:10.1016/j.compstruct.2022.115368.

[34] M. Rathnasabapathy, AP. Mouritz, AC. Orifici, Finite element modelling of the impact response of fibre metal laminates under tension preloading, Composites A 157 (2022) 101148, doi:10.1016/j.compositesa.2022.106930.

[35] M. Rathnasabapathy, AC. Orifici, AP. Mouritz, Impact damage to fibre metal laminates under compression loading, Compos. Commun. 32 (2022) 106930, doi:10.1016/j.coco.2022.101148.

[36] T. Mitrevski, IH. Marshall, RS. Thomson, R. Jones, Low-velocity impacts on preloaded GFRP specimens with various impactor shapes, Compos. Struct. 76 (2006) 209–217.

[37] CX. Wang, T. Suo, C. Hang, YL. Li, P. Xue, et al., Influence of in-plane tensile preloads on impact responses of composite laminated plates, Int. J. Mech. Sci. 161-162 (2019) 105012, doi:10.1016/j.ijmecsci.2019.105012.

[38] MV. Zhikharev, SB. Sapozhnikov, OA. Kudryavtsev, VM. Zhikharev, Effect of tensile preloading on the ballistic properties of GFRP, Composites B 168 (2019) 524–531, doi:10.1016/j.compositesb.2019.03.026.

[39] D. Schueler, N. Toso-Pentecôte, H. Voggenreiter, Effects of static preloads on the high velocity impact response of composite plates, Compos. Struct. 153 (2016) 549–556, doi:10.1016/j.compstruct.2016.06.062.

[40] AR. Moallemzadeh, SAR. Sabet, H. Abedini, Preloaded composite panels under high velocity impact, Int. J. Impact. Eng. 114 (2018) 153–159, doi:10.1016/j.ijimpeng.2017.12.019.

[41] ZJ. Ji, ZD. Guan, ZS. Li, RM. Tan, Effects of compressive preload on impact damage performance of composite laminates, Acta Mater. Compos. Sin. 33 (2016) 1677–1686, doi:10.13801/j.cnki.fhclxb.20151020.005.

[42] CY. Zhan, T. Liu, MN. Yuan, Influence of pre-stress on ballistic limit of kevlar fiber-reinforced composite laminate, Ordnance Mater. Sci. Eng. 42 (2019) 6–11, doi:10.14024/j.cnki.1004-244x.20190211.001.

[43] Z. Hashin, A. Rotem, Fatigue failure criterion for fiber reinforced materials, J. Compos. Mater. 7 (1973) 448–464, doi:10.1177/002199837300700404.

[44] Z. Hashin, Failure criteria for unidirectional fiber composites, J. Appl. Mech.-Trans. Asme 47 (1980) 329–334, doi:10.1115/1.3153664.

[45] Bažant ZdeněkP, BH. Oh, Crack band theory for fracture of concrete, Matér. Constr. 16 (1983) 155–177, doi:10.1007/BF02486267.

[46] PF. Liu, BB. Liao, LY. Jia, XQ. Peng, Finite element analysis of dynamic progressive failure of carbon fiber composite laminates under low velocity impact, Compos. Struct. 149 (2016) 408–422, doi:10.1016/j.compstruct.2016.04.012.

[47] JJ. Zhou, PH. Wen, SN. Wang, Finite element analysis of a modified progressive damage model for composite laminates under low-velocity impact, Compos. Struct. 225 (2019) 111113, doi:10.1016/j.compstruct. 2019.111113.

[48] ML. Benzeggagh, M. Kenane, Measurement of mixed-mode delamination fracture toughness of unidirectional glass/epoxy composites with mixed-mode bending apparatus, Compos. Sci. Technol. 56 (1996) 439–449, doi:10.1016/0266-3538(96)00005-x.

[49] D. Zhang, XT. Zheng, J. Zhou, WX. Zhang, Bridging the low-velocity impact energy versus impact damage and residual compression strength for composite laminates, J. Reinf. Plast. Comp. 40 (2020) 378–390, doi:10.1177/0731684420970643.

[50] YD. Zhou, YC. Sun, WC. Cai, Bird-striking damage of rotating laminates using SPH-CDM method, Aerosp. Sci. Technol. 84 (2019) 265–272, doi:10.1016/j.ast.2018.10.009.

[51] KM. Mikkor, RS. Thomson, I. Herszberg, T. Weller, AP. Mouritz, Finite element modelling of impact on preloaded composite panels, Compos. Struct. 75 (2006) 501–513, doi:10.1016/j.compstruct.2006.04.056.

Graphical abstract

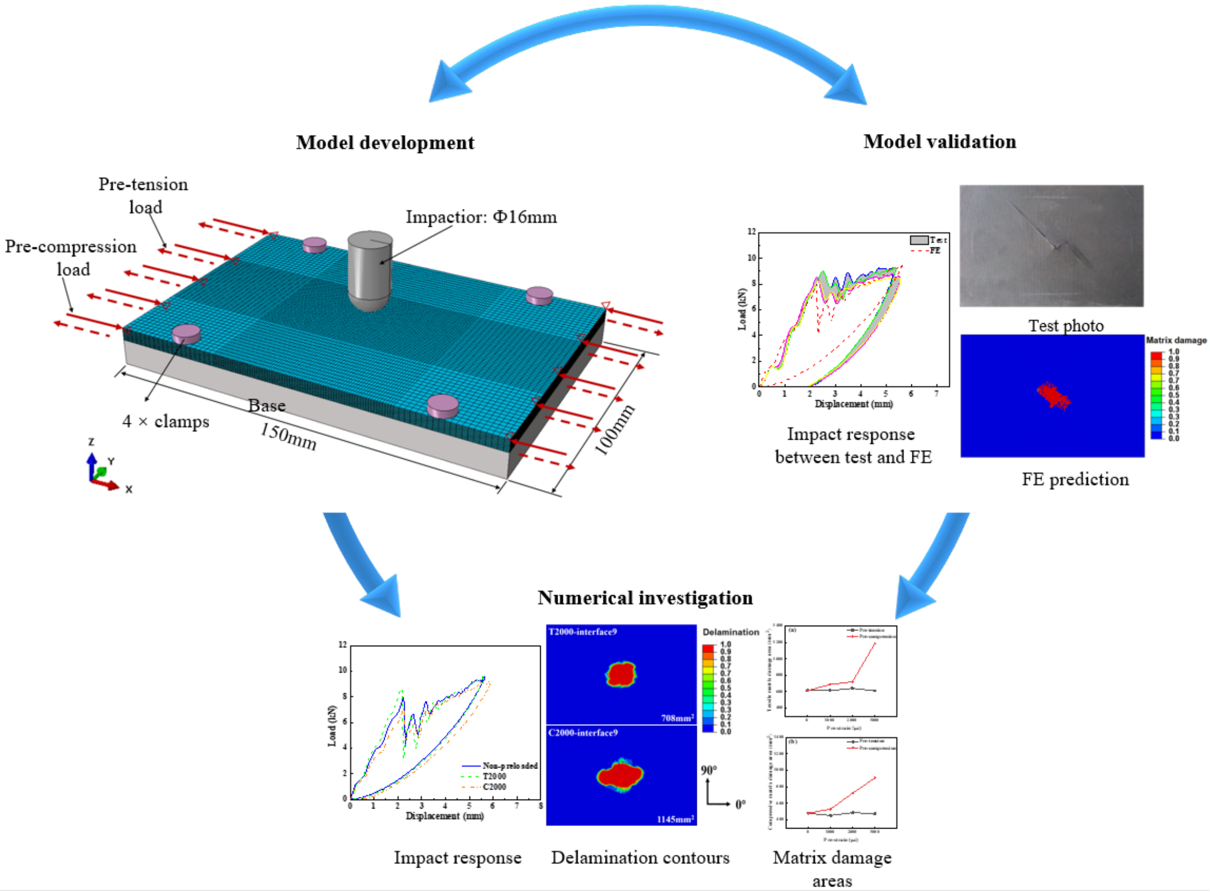

Highlights

- An impact damage model, with user-defined material subroutine, has been developed and validated for composite materials.
- The effect of pre-load on the damage mechanisms of composite laminates subjected to low velocity impact has been studied.
- Pre-compression load has an aggravative effect on the impact damage in the composite laminates, whereas pre-tension has much less such type of effect.
- The developed computational model is aimed to provide a guidance to the design and maintenance of composite structures subjected to pre-load.